Published in Computers & Geosciences 37, issue 11, 1825-1835, 2011
which should be used for any reference to this work

MWTmat—application of multiscale wavelet tomography on potential fields

Guillaume Mauri [a,*], Glyn Williams-Jones [a], Ginette Saracco [b]

[a] Department of Earth Sciences, Simon Fraser University, Burnaby, BC, Canada
[b] CNRS-CEREGE, Université P. Cézanne, Géophysique and Planétologie, Europole de l'Arbois, Aix-en-Provence, France

A B S T R A C T

Wavelet analysis is a well-known technique in the sciences to extract essential information from measured signals. Based on the theory developed by previous studies on the Poisson kernel family, this study presents an open source code, which allows for the determination of the depth of the source responsible for the measured potential field. MWTmat, based on the Matlab platform, does not require the wavelet tool box, is easy to use, and allows the user to select the analyzing wavelets and parameters. The program offers a panel of 10 different wavelets based on the Poisson kernel family and the choice between a fully manual and a semiautomatic mode for selection of lines of extrema. The general equations for both horizontal and vertical derivative wavelets are presented in this study, allowing the user to add new wavelets. Continuous wavelet analyses can be used to efficiently analyze electrical, magnetic, and gravity signals; examples are presented here. The MWTmat code and the multiscale wavelet tomography approach are an efficient method for investigating spatial and temporal changes of sources generating potential field signals.

Keywords
Wavelet, Signal processing, Potential field, Self-potential, Gravimetry, Geothermal

1. Introduction

Since the 1980s, continuous wavelet transforms have become an important tool for signal analyses. In the late 1990s, the ground-breaking work of Moreau et al. (1997, 1999) enhanced our understanding of the sources responsible for potential field signals (i.e., gravity, magnetism, and electricity) by creating the Poisson kernel family, which enables depth calculation of the source of the measured signal. While analyses based on traditional wavelets (i.e., Morlet, Mexican hat) became more widespread in the sciences (Grossmann and Morlet, 1984; Goupillaud et al., 1984; Tchamitchian, 1989, and references therein), the Poisson kernel family has had only limited use in geosciences for potential field data. However, numerous studies have shown the importance of the Poisson kernel family in both real and complex continuous wavelet transforms (e.g., Saracco, 1994; Moreau et al., 1997, 1999; Sailhac et al., 2000; Sailhac and Marquis, 2001; Fedi and Quarta, 1998; Martelet et al., 2001; Saracco et al., 2004, 2007; Boukerbout and Gibert, 2006; Cooper, 2006; Fedi, 2007; Mauri et al., 2010). In this study, the continuous wavelet transform was chosen over other techniques (e.g., wavenumber decomposition) because of its capacity to simultaneously perform multiscale analysis, depth determination, and homogeneous distribution of the source without a priori source information.

This study presents an open source user friendly Matlab code, MWTmat, for real and complex wavelet analyses on potential fields, which allows the user to locate the sources of electrical (self-potential), gravity, or magnetic signals. The code uses a panel of 10 different wavelets based on the Poisson kernel family that enables one to study the depth and structure coefficient of the source of analyzed signal (Fig. 1). The depth calculation method is based on a statistical approach, which allows one to both limit artifact depth and reinforce the localization and the homogeneous distribution of the source by cross-correlation of the calculations using different wavelets. A brief overview of the mathematical background of Poisson kernel family wavelets is presented along with examples from both synthetic and field studies of self-potential, magnetic, and gravity signals. Finally, the multiscale wavelet tomography (MWT) approach is discussed with its application to potential field source localization. In this study, we define complex analyses to be the result of the depth calculation on both the real and the imaginary values that result from the wavelet analyses.

2. Continuous wavelet transform

The continuous wavelet transform (CWT), $L_{(b,a)S}$, is the conversion of any signal into a matrix made of a sum of scalar products in Fourier space, which can be seen as how well the signal matches the analyzing wavelet (Fig. 1). As both analyzed signal and analyzing wavelet have their own signature (e.g., shape, structure, and amplitude), the analyses of the first by the second give a unique signature, which allows characterization of the

* Corresponding author. Current address: Laboratoire Suisse de Géothermie—CREGE, Université de Neuchâtel, Neuchâtel, Switzerland.
E-mail address: guillaume.mauri@unine.ch (G. Mauri).

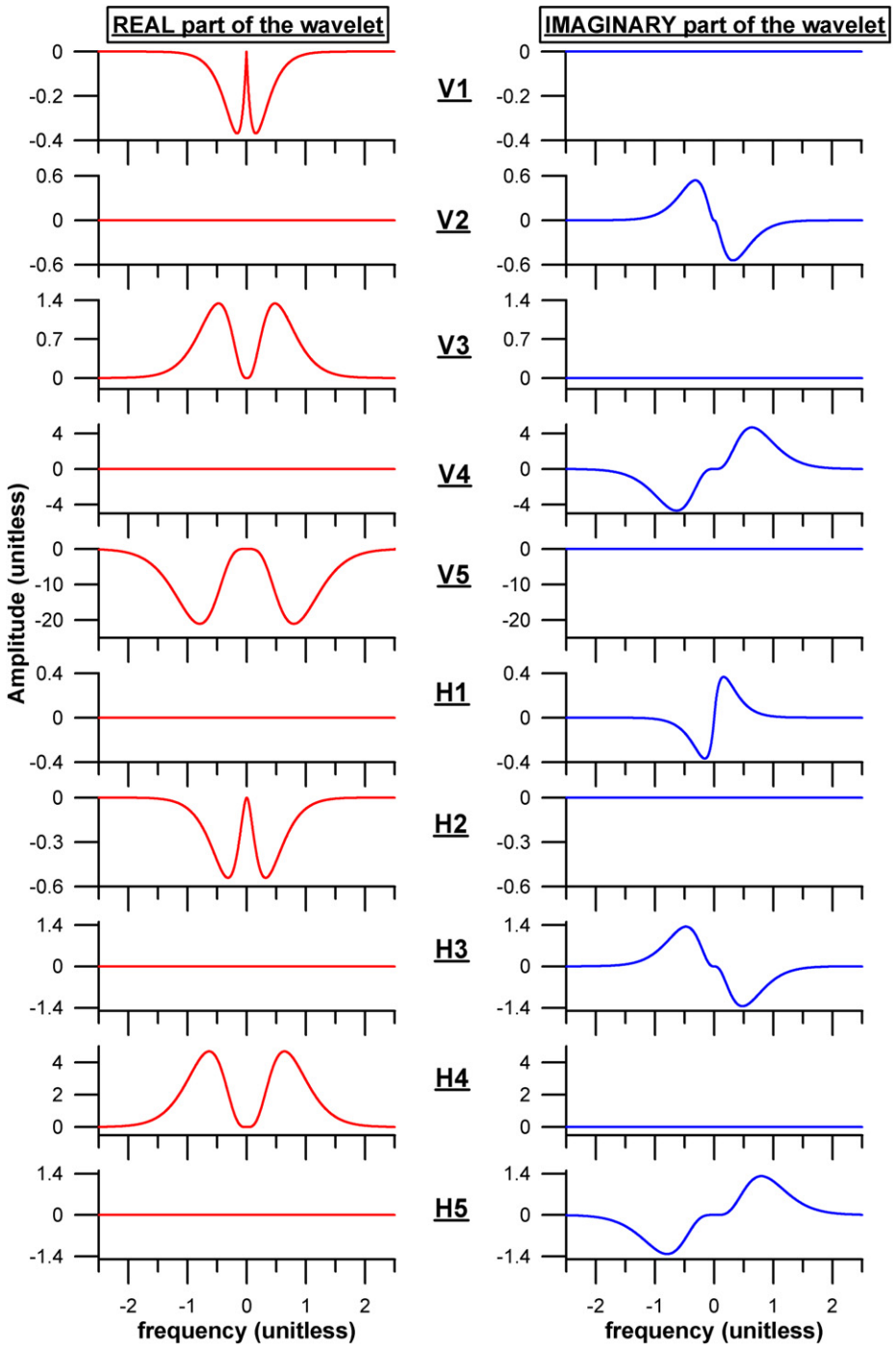

Fig. 1. Poisson kernel wavelet family in Fourier space with their real and imaginary parts. V1 to V5 are the vertical derivatives of order from 1 to 5. H1 to H5 are the horizontal derivatives of order from 1 to 5. Each wavelet is calculated over 1024 points on a frequency from 0 to 2.5 at a dilation $a=1$. The negative part of the frequency axis is the symmetrical construction to give the wavelet its full shape.

structure of the analyzed signal (e.g., frequency content and structure; Fig. 2). The mathematical expression of the wavelet transform, $L_{(b,a)}$, for a signal, s, by a wavelet, g, can be described as follows (Grossmann and Morlet, 1984; Moreau et al., 1997):

$$L_{(b,a)s} = a^{-\gamma} \int_X g_n([x\text{-}b]/a)s(x)dx^{\gamma} \quad \text{with} \quad q = n+\gamma+a, \tag{1}$$

where the dimension order of the space, $\gamma \in N$, b is the translation parameter, and a the dilation parameter; this allows the analyzing wavelet to act as a band filter. The order of the derivative, $n \in N$, signal s has a homogeneous distribution order, $\alpha \in N$, and size of the signal, $x \in N$. X represents the number of elements making the analyzed signal.

These studies apply the CWT within the frequency domain, rather than within the spatial domain, for increased efficiency. Within the frequency domain, the general equation of the horizontal derivative of order n of the Poisson kernel family, $H_n(u)$ (Moreau et al., 1997, 1999; Saracco et al., 2004), is

$$H_n(u) = (2\pi u)^n \exp(-2\pi|u|), \tag{2}$$

with u the wavenumber of the spatial variable, x, in the frequency domain and n being the order of the derivative, such as $n \in N$.

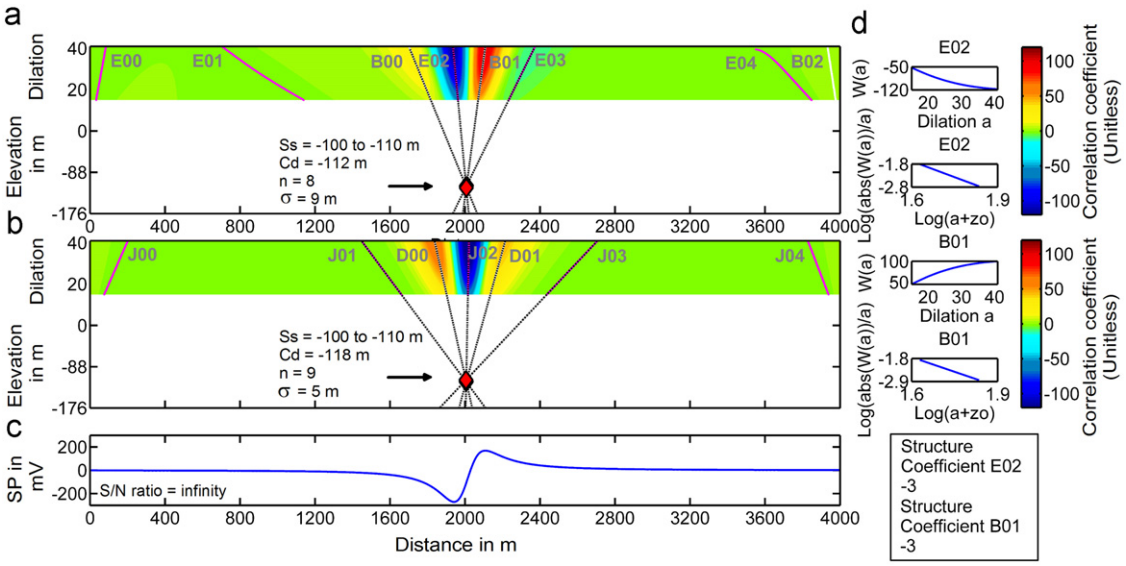

Fig. 2. Continuous wavelet analysis with the third vertical derivative (V3) of one dipole at a depth, $z=-100$ m. Analyses were made with 500 dilations in a range from 15 to 41. (a) Real value of the analyses. The depth calculations (red diamonds) are based on 8 solutions. E00 to E04 and J00 to J04 are extrema of maximum coefficient correlation. B00 to B02 and D01 to D01 are extrema of lowest coefficient correlation. (b) Imaginary value of the analyses. The depth calculations (red diamonds) are based on 9 solutions. (c) Self-potential signal with no noise (SNR=infinity) and a sampling step of 1 m represents the dipole generating the electrical signal. (d) The four diagrams represent the selected extrema lines used for the depth determination to determine the structure coefficient of the dipole source. A model of the synthetic self-potential signal is presented in Fig. 4. Ss is the synthetic signal depth, Cd is the calculated depth, and σ is one standard deviation. (For interpretation of the references to color in this figure legend, the reader is referred to the web version of this article.)

Similarly, through the Hilbert transform of the horizontal derivative, the general equation of the vertical derivative of order n of the Poisson family, $V_n(u)$, is

$$V_n(u) = -2\pi|u|(2\pi iu)^{(n-1)}\exp(-2\pi|u|), \tag{3}$$

with u the wavenumber of the spatial variable, x, in the frequency domain.

As described in previous studies (e.g., Moreau et al., 1997), potential field signals analyzed by any of these wavelets (V_n, H_n) allow for estimation of both depth, z, and homogeneous distribution order, α, of the source generating the analyzed signal. Source depth is calculated through the intersection of the converging extrema lines (Fig. 2). To do it accurately, the analyzing wavelet must have a derivative order, n, greater than the homogeneous distribution of source, α, such as (Moreau et al., 1997; Saracco et al., 2007; Mauri et al., 2010, and references therein)

$$n \geq -(1+\alpha). \tag{4}$$

The homogeneous distribution of the source also depends on the dimension of the space in which the signal is analyzed. In 2D space for a self-potential or magnetic signal, homogeneous distribution of a detected singularity by MWT may represent dipoles ($\alpha=-3$) or monopoles ($\alpha=-2$). Previous studies have shown that water flow can be considered to behave as a monopole or a dipole when its capacity to generate electricity is investigated (Moreau et al., 1997; Saracco et al., 2004; Mauri et al., 2010). In the case of a gravity signal, the homogeneous distribution of a detected singularity represents the shape of the source (e.g., sphere, $\alpha=-2$; Martelet et al., 2001; Fedi, 2007). A magnetic dipole has a homogeneous distribution ($\alpha=-3$). The homogeneous distribution is determined from the slope of the extrema lines converging toward the source (Fig. 2). In this study, the analyzed sources have a homogeneous distribution of $\alpha=-3$ or smaller and the wavelets used are therefore of order $n=2$ (wavelets V2 and H2) or $n=3$ (wavelets V3 and H3), as described in Eq. (4) (Mauri et al., 2010).

3. MWTmat code overview

The multiscale wavelet code, MWTmat, is separated into two programs. The first, MWTmat_Analysis.m, includes the wavelet equations, the continuous transform, and the extrema filter. The second, MWTmat_Depth.m, includes the linear regression, depth calculation, and the structure coefficient calculation. A flow diagram of the code structure for each file is presented in Fig. 3.

In order to assure that each CWT is properly performed, the MWTmat code includes a number of restrictions. The most important is that the Nyquist–Shannon theorem be respected, so that the wavelet is always well defined within the range of selected dilation. Each wavelet is well defined on a predetermined support based on the dilation, $a=1$ (Fig. 1), which is also the smallest dilation that can be selected with the code. For higher dilation, the MWTmat code will display the maximum dilation possible based on the data length of the analyzed input profile.

MWTmat can also perform complex wavelet analyses (Fig. 2b) in addition to the real wavelet analyses (Fig. 2a). In complex mode, the depth and homogeneous distribution order of the source can be calculated on either the imaginary correlation coefficient or the phase matrix resulting from the complex continuous wavelet analyses.

Depth calculations can be performed through an automatic or semiautomatic linear regression mode. In the latter, the user has the option to decide what section of each extrema best represents it, prior to the determination of the linear regression. For each depth calculation of a source, the associated homogeneous distribution order is determined from the selected extrema line and the calculated depth intersects (Fig. 2d, e.g., magnetic signal, Table 4). A full description of the code can be found in the Supplementary data.

4. Multiscale wavelet tomography

The multiscale wavelet tomography is based on a statistical approach of continuous wavelet analyses using the Poisson kernel

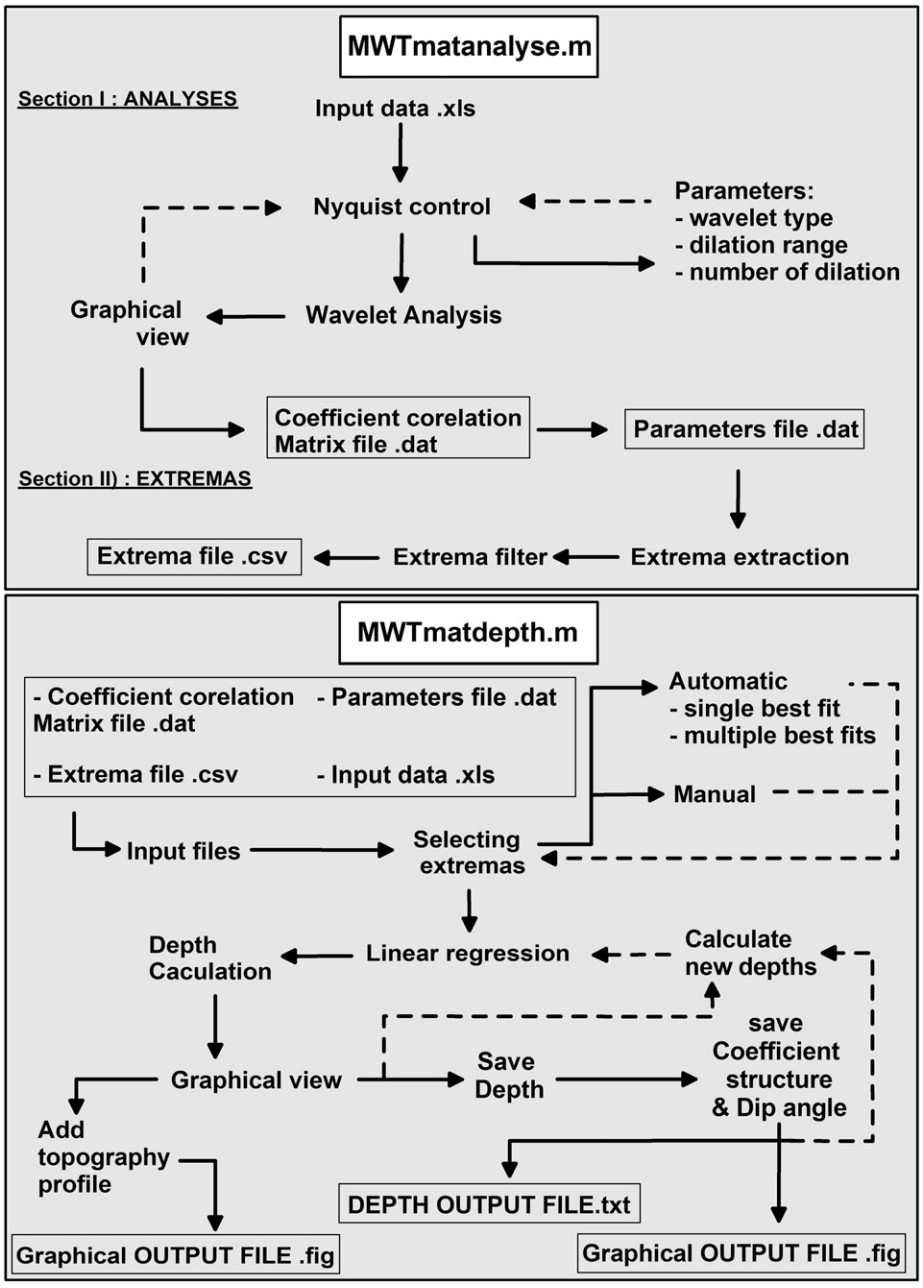

Fig. 3. Flow diagram highlighting the execution order of the MWTmat code. Solid lines represent forward processes, while broken lines show feedback processes. The white boxes represent the MWTmat code associated with each process.

family. Previous studies have shown that noise is the strongest source of error on depth analyses (Mauri et al., 2010). Furthermore, even though all the wavelets from the Poisson kernel family are very similar in shape (Fig. 1), each has its own center frequency, making them react slightly differently to the same signal and thus to the same noise. Even though the law of the derivative order can help determine the most appropriate wavelet for analysis of a signal, there is no objective way to determine which wavelet will best characterize the analyzed signal. Therefore, to avoid user uncertainty and the risk of depth artifacts, the MWT approach uses at least four wavelets from the Poisson kernel family and considers only depths, which are characterized by at least three of the four analyzing wavelets. The more the wavelets used, the higher the capacity to accurately localize the source generating the main anomaly.

5. Application and depth accuracy

5.1. Synthetic self-potential signal

A synthetic example of self-potential data was generated for a dipole present within a nonhomogeneous ground having a large contrast in ground resistivity (Fig. 4). The dipole is a cylinder 300 m long and 60 m wide, tilted at 20°. The top edge of the dipole is 257 m below the topographic surface on its center (Fig. 4). The ground resistivity contrast is 3 orders of magnitude, with one layer at 50 kΩ and another at 10,000 kΩ. The topographic surface has a slope of 10°. In addition, a 10% Gaussian noise (signal to noise ratio, SNR, of 10) has been applied on the total field signal, which has a 4 m sampling step (Fig. 4).

Each analysis was made over a range of dilation from 15 to 25 with 500 dilations. Multiscale wavelet analyses of the synthetic

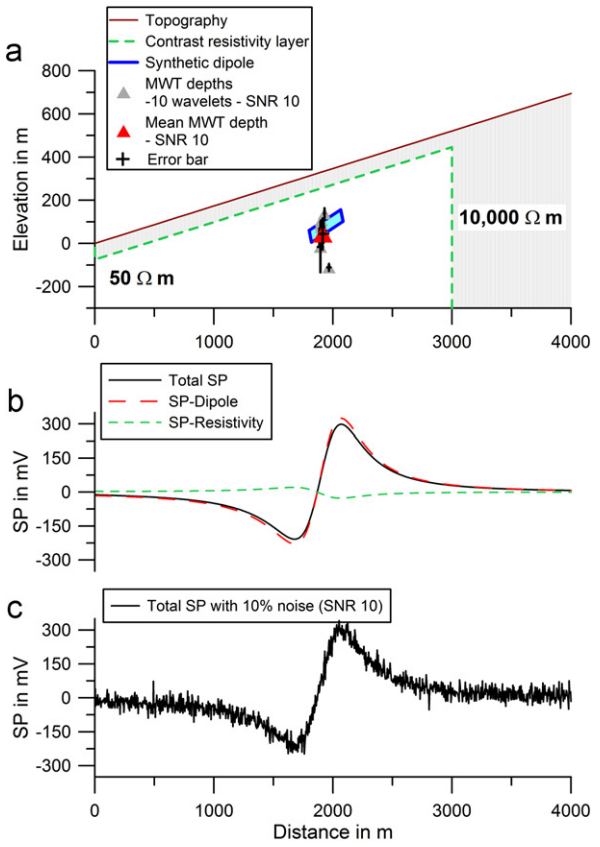

Fig. 4. 2D model of a synthetic self-potential signal generated by a dipole (20°) in a non-uniform medium. Grid sampling step is 4 m. (a) Model used to generate self-potential signal over a 10° topography slope. Interface between two mediums of differing resistivity is represented by a resistivity contrast layer (green dashed line). The dipole (300 m × 60 m; blue rectangle), tilted at 20°, has its upper left corner 250 m below topographic surface. Gray triangles are the mean depths of all wavelets. The red triangle represents the mean depth based on the statistical approach using all the results. Error bars for the statistical mean depth are 1 sigma. Results are presented in Table 1. (b) Synthetic self-potential signal associated with the model: resistivity contrast layer component (green dashed line), SP signal generated by the dipole (red dashed line), and total SP signal (solid black line). (c) Total SP signal presented in b with 10% Gaussian noise (SNR = 10). Ss is the synthetic signal depth, Cd is the calculated depth, and σ is one standard deviation. (For interpretation of the references to color in this figure legend, the reader is referred to the web version of this article.)

self-potential signal were performed with 10 wavelets (Fig. 1). Normally, since the synthetic signal source is a dipole, and following the law of derivative order (Eq. (4)), only wavelets having a derivative order greater than 2 should be used. However, in order to show the importance of both this law and the statistical approach, the first derivative order has also been used to calculate the dipole depth (Table 1). Each depth from each wavelet analysis has been calculated based on a range from 26 to 82 solutions. The maximum depth error reaches 74% (gray triangles in Fig. 4a; Table 1), while the data scattering is generally less than 20%, with a maximum of 47% (for a SNR 5). When using the MWT approach based on all the wavelet analyses, the mean depth error is less than 16% for a SNR lower than 10 (Table 1, red triangle in Fig. 4a) and of 24% for a SNR of 5. The depths scattering represented by the sigma error is 47% for a SNR of 5. The greatest error is obtained with the wavelet of first derivative order (H1, V1; Table 1), which is the wavelet that does not follow the rules set through Eq. (4). The wavelet analyses can also determine both structural coefficient (dipole, $\alpha = -3$) and dip angle (Table 1).

5.2. *Stromboli volcano self-potential signal*

Stromboli volcano, in the Tyrrhenian Sea, Italy, is a stratovolcano in the northern part of the Aeolian archipelago (Gillot and Keller, 1993; Fig. 5a). The volcanic stratigraphy presents a large variation of ground resistivity (<100 to $>3000\,\Omega$ m) and the edifice hosts a well-established hydrothermal system in the summit area (Finizola et al., 2006, and references therein). Previous work on multiscale wavelet tomography of self-potential data located the depth of the hydrothermal system in the same area and similar depth as other independent subsurface models (Mauri et al., 2010; Fig. 6; Table 2). Hydrothermal fluids are found within the lowest resistivity layer and their depths have been located near the surface; the top of the main hydrothermal flow is located ~100 m beneath the Pizzo, the summit of Stromboli, as well as further southwest (Table 2; Fig. 6; Mauri et al., 2010). Along the lower northeast flank of Stromboli, where underground water flow is present (Finizola et al., 2006), the associated water table was located at ~180 m beneath the surface (Fig. 6; Table 2). The multiscale wavelet tomography of self-potential data gives reliable depths on Stromboli volcano and has been shown by independent modeling to match existing structures. The depth scattering ranges between 15 and 65 m and constrains the main water flow responsible for the measured self-potential anomalies.

Table 1
Results of depth calculation for each of the synthetic signals by 10 different wavelets.

Signal	Wavelet type	SNR	Solution	Unit in m				Error in %				Coefficient structure	Dip angle in deg.
				Distance z	σx	Depth z	σz	x	σx	z	σz		
Statistical approach on electrical signal													
Ss	–	–	–	1932	–	0–156	–	–	–	–	–	−3	20
Cd	10	∞	605	1917	8	43	19	1	0	14	7	−3	16
Cd	10	10	451	1913	28	44	72	1	1	13	28	−3	14
Cd	10	5	427	1906	35	17	122	1	2	24	47	−3	12
Individual analyses													
Ss	–	–	–	1932	–	0–156	–	–	–	–	–	−3	20
Cd	H1	∞	56	1912	3	41	12	1	0	14	5	−3	15
Cd	H2	∞	82	1911	4	40	16	1	0	15	6	−3	15
Cd	H3	∞	56	1919	9	49	23	1	0	11	9	−3	16
Cd	H4	∞	60	1911	6	30	14	1	0	19	5	−3	17
Cd	H5	∞	63	1918	8	25	14	1	0	21	5	−3	20
Cd	V1	∞	56	1914	3	43	15	1	0	14	6	−3	15
Cd	V2	∞	57	1921	7	61	14	1	0	7	5	−3	15
Cd	V3	∞	57	1922	6	55	17	1	0	9	7	−3	16
Cd	V4	∞	59	1922	6	48	16	1	0	12	6	−3	16
Cd	V5	∞	59	1926	10	39	20	0	1	15	8	−3	19
Cd	H1	10	29	1967	13	−111	16	2	1	74	6	−4	14

Table 1 (*continued*)

Signal	Wavelet type	SNR	Solution	Unit in m				Error in %				Coefficient structure	Dip angle in deg.
				Distance *z*	*σx*	Depth *z*	*σz*	*x*	*σx*	*z*	*σz*		
Cd	H2	10	54	1922	21	58	54	1	1	8	21	−3	12
Cd	H3	10	26	1900	1	91	0	2	0	5	0	−2	12
Cd	H4	10	52	1906	3	76	26	1	0	1	10	−3	9
Cd	H5	10	54	1885	7	32	38	2	0	18	15	−4	16
Cd	V1	10	52	1895	22	−16	117	2	1	37	46	−3	15
Cd	V2	10	26	1903	1	107	0	2	0	11	0	−2	13
Cd	V3	10	26	1902	1	88	0	2	0	4	0	−3	12
Cd	V4	10	54	1930	4	139	25	0	0	24	10	−2	22
Cd	V5	10	78	1926	34	45	35	0	2	13	14	−2	14
Cd	H1	5	54	1950	33	−57	171	1	2	53	67	−4	15
Cd	H2	5	54	1921	26	30	108	1	1	19	42	−3	12
Cd	H3	5	26	1899	1	90	0	2	0	5	0	−2	12
Cd	H4	5	27	1909	2	130	0	1	0	20	0	−2	9
Cd	H5	5	80	1874	21	−6	84	3	1	33	33	−4	7
Cd	V1	5	53	1891	19	−54	187	2	1	51	73	−3	13
Cd	V2	5	26	1897	1	132	0	2	0	21	0	−2	11
Cd	V3	5	26	1901	0	94	0	2	0	6	0	−3	10
Cd	V4	5	28	1937	6	46	4	0	0	12	2	−3	12
Cd	V5	5	53	1900	47	−15	36	2	2	36	14	−4	15

Synthetic dipole model is described in Fig. 4. Ss is the synthetic signal depth, Cd is the calculated depth, SNR is the signal to noise ratio, and σ is one standard deviation.

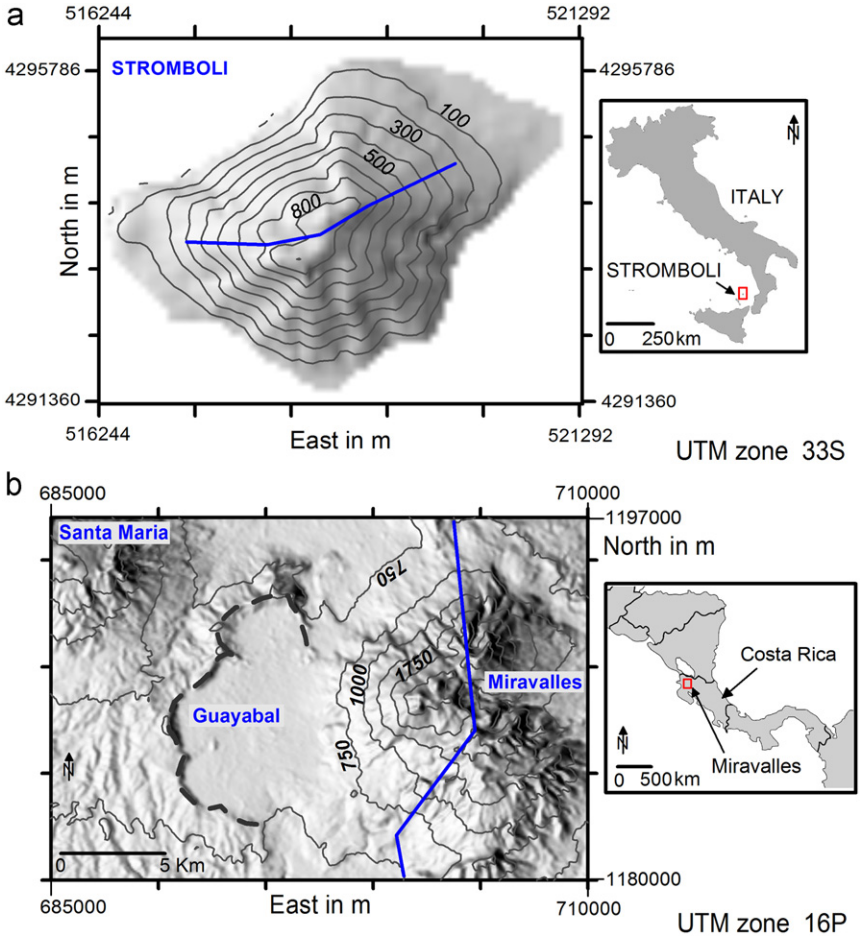

Fig. 5. (a) Stomboli volcano, Italy. The blue line represents the self-potential profile shown in Fig. 6. (b) Miravalles volcano, Costa Rica. The blue line represents the gravity profile shown in Fig. 9. (For interpretation of the references to color in this figure legend, the reader is referred to the web version of this article.)

5.3. *Synthetic magnetic signal*

A synthetic magnetic signal was generated from a 3D model of a dike using Mag3D (Li and Oldenburg, 1998). The dike is 120 m long, 40 m thick, 40 m wide, and titled at 35° (Fig. 7a). Complex wavelet analyses were applied to the synthetic magnetic signal with three different levels of Gaussian noise (0%, 10%, and 20%). The noisy synthetic signals were analyzed with 6 different

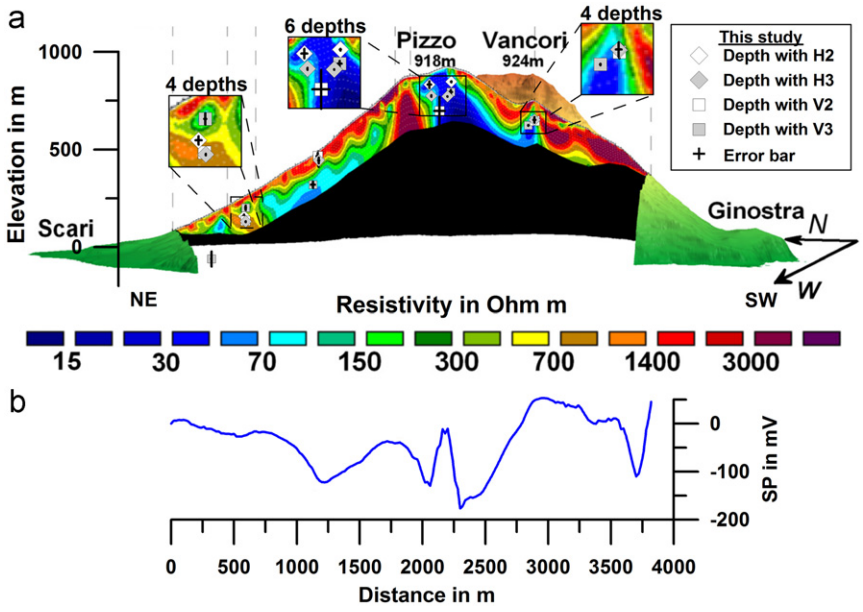

Fig. 6. Multiscale wavelet tomography of a self-potential signal on Stromboli volcano, Italy, generated by groundwater flow. (a) Comparison between MWT-calculated depths of hydrothermal fluids (squares and diamonds) and electrical resistivity model (Finizola et al., 2006). V2, V3, H2, and H3 are the second and third order of the vertical and horizontal derivatives (Mauri et al., 2010). Error bars represent one standard deviation, see Table 2. (b) Self-potential profile across the summit of Stromboli (see Fig. 5a). Modified from Mauri et al. (2010) and Finizola et al. (2006).

Table 2
Source depths calculated by multiscale wavelet tomography of self-potential profiles on Stromboli volcano (Fig. 6).

Signal	Number of wavelets	Solution	x	σx	z	σz	Elevation asl
Cd	4	16	1160	22	−66	26	427
Cd	2	4	2060	10	−80	38	806
Cd	4	8	2200	43	−130	46	788
Cd	4	16	2880	25	−105	17	643
Cd	4	9	590	7	−184	62	105

Number of wavelets used in MWT calculations to locate source depths and position along profile. Distance along profile (x), depth (z), and elevation are in m. σ is one standard deviation. Modified from Mauri et al. (2010).

wavelets: the second, third, and fourth vertical and horizontal derivatives (V2, V3, V4, H2, H3, and H4; Fig. 1). Each analysis was made over a range of dilation from 15 to 25 with 500 dilations. On the magnetic signal without noise, the results show that the mean calculated depth has only 5% error from the mean depth of the modeled dike, with a sigma error of 5%. A summary of analyses for each of the synthetic magnetic signals is presented in Table 3. Noise does not significantly affect the error on the mean depth, which is always less than 10% vertical error (Table 3). However, stronger noise increases the data scattering, which reaches 60% for 20% Gaussian noise (Fig. 7). Thus, on magnetic signals, the MWT can give both reliable depth information and structure coefficients of the source generating magnetic anomaly (Table 3).

5.4. *Synthetic gravity signal*

A synthetic gravity signal was generated from a 3D model of a sphere using Grav3D (Li and Oldenburg, 1998). The sphere is 60 m in diameter, with its center at 110 m below a flat topography (Fig. 8). The density contrast between the sphere and its surroundings is 3 g cm^{-3}. On the synthetic gravity signal (Fig. 8b),

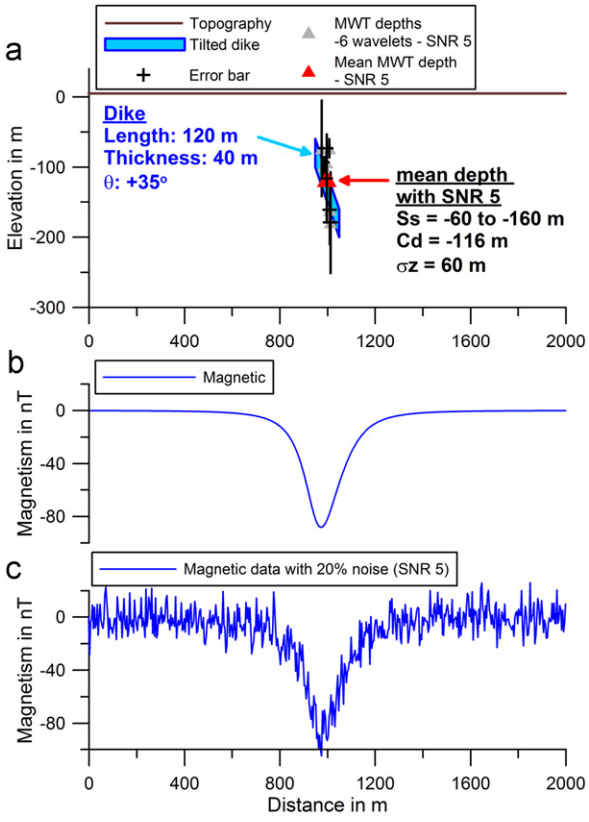

Fig. 7. (a) 3D model of a synthetic magnetic signal generated by a tilted dike and affected by 20% noise (SNR=5). Grid sampling step is 4 m. Topography is flat. The yellow diamond represents the mean depth calculated with the MWT using 6 wavelets (Table 3). (b) Synthetic magnetic signal associated with the model. (c) Magnetic signal presented in (b) with a 20% Gaussian noise (SNR=5). Ss is the synthetic signal depth, Cd is the calculated depth, and σz is one standard deviation. (For interpretation of the references to color in this figure legend, the reader is referred to the web version of this article.)

Table 3
Source depths calculated by multiscale wavelet tomography of synthetic magnetic profiles generated by a tilted dike (Fig. 7).

Signal	Number of wavelet	SNR	Solution	Unit (m)				Error (%)				Structure coefficient	Dip angle in deg. [180]
				Distance *x*	*σx*	Depth *z*	*σz*	*x*	*σx*	*z*	*σz*		
Statistical approach on magnetic signal													
Ss	–	–	–	948–1048	–	−60 to −160	–	–	–	–	–	−3	35
Cd	6	∞	328	981	9	−100	5	2	1	5	5	−3	−143
Cd	6	10	292	986	9	−104	15	1	1	1	14	−3	−135
Cd	6	5	292	996	22	−116	63	0	2	10	60	−3	−133
Individual analyses													
Ss	–	–	–	948–1048	–	−60 to −160	–	–	–	–	–	−3	35
Cd	H2	∞	54	979	8	−99	5	2	1	−6	−5	−3	−142
Cd	H3	∞	55	974	7	−99	6	3	1	−6	−6	−3	−145
Cd	H4	∞	55	980	8	−101	5	2	1	−4	−5	−3	−147
Cd	V2	∞	54	979	8	−99	5	2	1	−6	−5	−3	−142
Cd	V3	∞	55	986	9	−101	5	1	1	−4	−5	−3	−137
Cd	V4	∞	55	986	9	−101	5	1	1	−4	−5	−3	−147
Cd	H2	10	28	1001	11	−79	11	0	1	−25	−10	−3	−134
Cd	H3	10	54	981	2	−99	4	2	0	−6	−4	−3	−132
Cd	H4	10	52	981	1	−117	6	2	0	−11	−6	−3	−136
Cd	V2	10	54	994	10	−91	12	1	1	−13	−11	−3	−135
Cd	V3	10	52	982	1	−111	4	2	0	−6	−4	−3	−136
Cd	V4	10	52	983	3	−117	12	2	0	−11	−11	−4	−134
Cd	H2	5	28	1007	13	−73	13	1	1	−30	−12	−2	−134
Cd	H3	5	54	985	1	−98	13	2	0	−7	−12	−3	−134
Cd	H4	5	52	1012	28	−179	72	1	3	−70	−69	−4	−132
Cd	V2	5	54	995	9	−93	14	1	1	−11	−13	−3	−134
Cd	V3	5	52	1009	26	−161	49	1	3	−53	−47	−4	−131
Cd	V4	5	52	975	11	−73	68	3	1	−30	−65	−3	−135

Name of wavelets used in MWT calculations to locate source depths and position along profile (Fig. 1). Distance along profile (*x*), depth (*z*), and elevation are in m. Ss is the synthetic signal depth, Cd is the calculated depth, and *σ* is one standard deviation. Results were obtained using both real and imaginary part of the MWT analyses.

three different levels of Gaussian noise were added (0%, 10%, and 20%); generally, field data do not show more than 10% noise (see field example below). The noisy synthetic signal was analyzed with four different wavelets: the fourth and fifth vertical derivatives (V4 and V5; Fig. 1) and the fourth and fifth horizontal derivatives (H4 and H5; Fig. 1). Analyses were made over a range of dilation from 20 to 35 with 600 dilations. Results on the noise-free gravity signal show that the mean depth has only 6% error from the mean depth of the modeled sphere, with a sigma error of 5% (Table 4). Fig. 8a shows the mean depth and its associated error (scattering of the data) for the analyzed signal with 20% noise. Noise does not significantly affect the error on the mean depth, which is always less than 10% vertical error (Table 4). However, stronger noise increases the scattering, which reaches 48% for 20% Gaussian noise. Thus, multiscale wavelet tomography on gravity signals can give reliable depth information on the source generating a gravity anomaly.

5.5. *Miravalles gravity signal*

Miravalles volcano, northwestern Costa Rica, is a stratovolcano, within the Guayabal caldera complex (Hallinan and Brown, 1995; (Fig. 5b). While Miravalles volcano has had no historic eruptions, it hosts a well-established geothermal system, which is used for geothermal energy production. The underground structure of Miravalles volcano hosts a feeding dyke (intermediate intrusion; Fig. 9) within the main cone, which is connected to a large and deeper structure. This intermediate intrusion is believed to be intruded by a pipe-shaped dense intrusion. Further north, the volcano-sediment unit and lava flows are vertically shifted along a fault (Hallinan and Brown, 1995; Fig. 9).

The gravity profile was analyzed with six different wavelets: the third to fifth vertical (V3, V4, and V5) and horizontal derivatives (H3, H4, and H5; Fig. 1), respectively. Analyses were performed over a range of dilation from 10 to 35 with 500

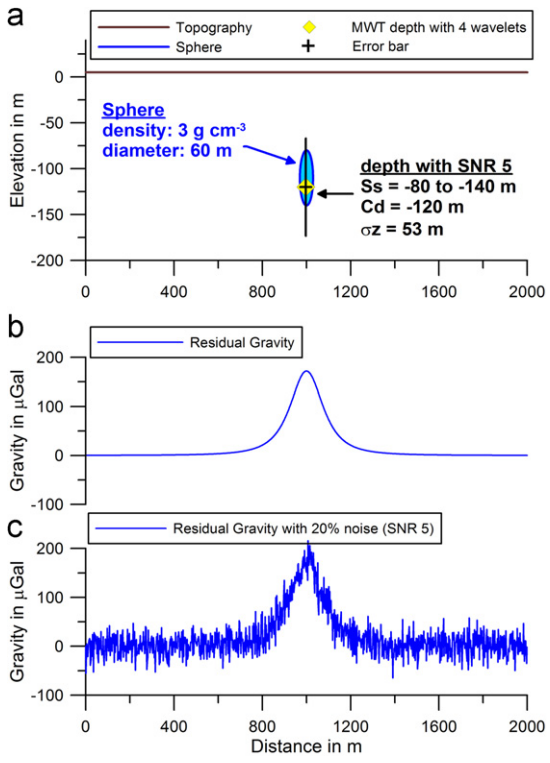

Fig. 8. (a) 3D model of a synthetic gravity signal generated by a sphere. Density contrast is 3 g cm^{-3} between the sphere and the surrounding homogeneous medium. Sampling step of the grid is 1 m. Topography is flat. The yellow diamond represents the mean depth calculated with the MWT using 6 wavelets (Table 4). (b) Synthetic gravity signal associated with the model. (c) Total gravity signal presented in (b) with a 20% Gaussian noise (SNR=5). Ss is the synthetic signal depth, Cd is calculated depth, and *σ* is one standard deviation. (For interpretation of the references to color in this figure legend, the reader is referred to the web version of this article.)

Table 4
Source depths calculated by multiscale wavelet tomography of synthetic gravity profiles generated by a sphere (Fig. 8).

Wavelet type	SNR	Solution	Unit (m)				Error (%)				Coefficient structure
			Distance x	σx	Depth z	σz	x	σz	z	σz	
–	–	–	970–1030	–	−80 to −140	–	–	–	–	–	−1
H4,H5,V4,V5	∞	321	1001	2	−103	5	0	0	6	5	−1
H4,H5,V4,V5	10	242	1002	15	−105	33	0	2	5	30	−1
H4,H5,V4,V5	5	214	997	25	−120	53	0	3	9	48	−1

Name of wavelets used in MWT calculations to locate source depths and position along profile (Fig. 1). Distance along profile (x), depth (z), and elevation are in m. σ is one standard deviation.

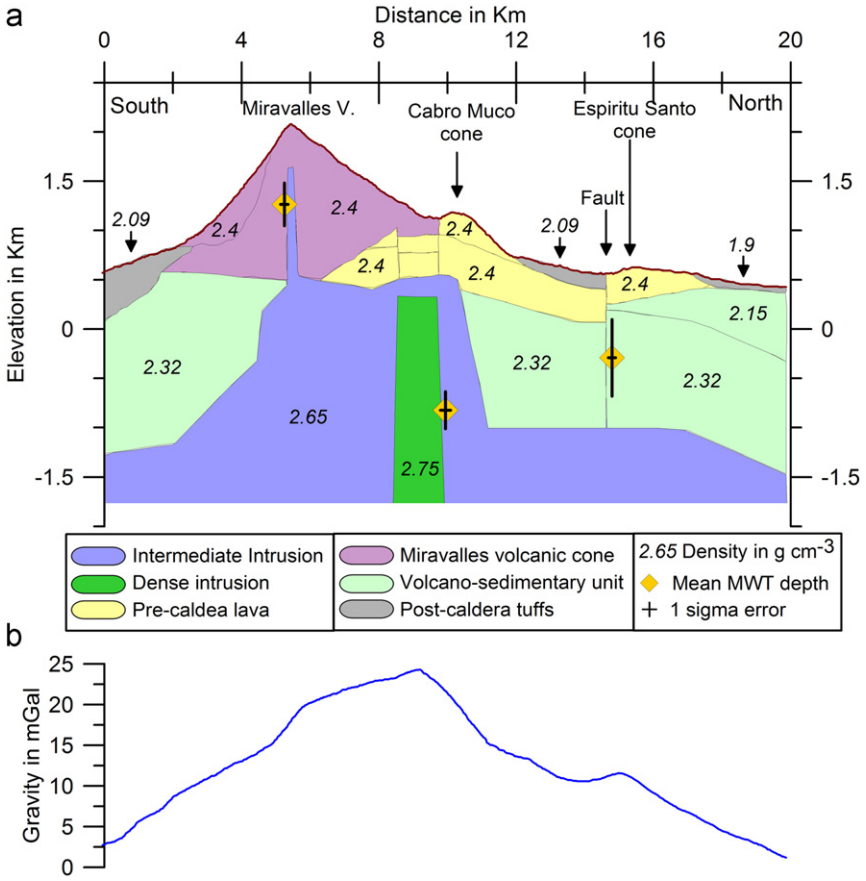

Fig. 9. Comparison between calculated depths and the subsurface model of Miravalles volcano, Costa Rica. (a) Modeled subsurface structures. Yellow diamonds represent mean depth of MWT analyses using six wavelets (V3, V4, V5 and H3, H4, H5). Error bar (1σ error) represents the data scattering. (b) Gravity profile in mGal (Fig. 5b). Full results are presented in Table 5. Modified from Hallinan and Brown (1995). (For interpretation of the references to color in this figure legend, the reader is referred to the web version of this article.)

dilations. Results from the multiscale wavelet tomography allow us to characterize three main structures (Table 5; Fig. 9), which are found along the main areas of density contrast: the edge of the feeding dike of the intermediate intrusion, the pipe-shaped dense intrusion, and the fault structure. Mean depths were calculated and compared to the mean vertical elevation of the associated structures. When only one wavelet is used to calculate the depth, the error can be $>100\%$; however, when numerous wavelets are used, the maximum error on the mean depth is 26% (Table 5) and the data scattering is 39%. The main limitation on the depth accuracy to locate the vertical center of the main density contrast limit is the ground complexity. The larger the geological object (e.g., dike and magmatic chamber), and the lower the density contrast between them, the lower the accuracy of the multiscale analyses.

6. Discussion and conclusion

MWTmat is an open source code in Matlab allowing for both real and complex continuous wavelet analyses on potential fields (gravity, magnetism, and self-potential) using wavelets from the Poisson kernel family. Multiscale wavelet tomography uses multiple analyses with different wavelets, reduces the risk of user error, and increases the confidence on the depth determination of the main source generating the measured signal. When used with

Table 5
Source depths calculated by multiscale wavelet tomography of the residual gravity profile on Miravalles volcano, Costa Rica (Fig. 9).

Mean depth	Number of		In m		*Z* in m below surface		Error on depth calculation		
	Wavelet	Solution	*x*	*σx*	Model Depth	Calculated Depth	*σz*	*z* (%)	*σz* (%)
Miravalles feeding dyke	6	162	5247	114	−1015	−749	216	26	21
Dense intrusion	3	81	9941	176	−2149	−1972	187	8	9
Volcano-sediment unit	6	161	14,791	108	−991	−858	388	13	39
Depth by wavelet	**Wavelet**	**Solution**	**In m**				**Error in %**		**In m asl**
			x	*σx*	*Z* asl	*σz*	*z*	*σz*	Topography
Miravalles feeding dyke									
Cd	H3	27	5178	15	1480	17	50	2	1991
Cd	H4	27	5192	8	1296	32	31	3	1998
Cd	H5	27	5394	6	1159	30	10	3	2073
Cd	V3	27	5224	10	1572	27	57	3	2011
Cd	V4	27	5114	5	939	52	0	5	1951
Cd	V5	27	5379	2	1152	12	10	1	2064
Dense intrusion									
Cd	H4	27	9801	10	−714	68	81	7	1122
Cd	V3	27	9883	12	−1072	74	118	7	1143
Cd	V4	27	10,139	10	−684	26	84	3	1183
Volcano-sediment unit									
Cd	H3	27	14,593	11	176	28	62	3	562
Cd	H4	27	14,813	16	−45	102	40	10	564
Cd	V4	27	14,780	5	102	25	54	2	568
Cd	V3	26	14,783	17	−548	99	10	10	567
Cd	V5	27	14,893	12	−711	50	26	5	568
Cd	H5	27	14,884	3	−734	30	28	3	568

Name of wavelets used in MWT: the third, fourth, and fifth vertical derivative wavelets (V3, V4, and V5; Fig. 1) and the third, fourth, and fifth horizontal derivative wavelets (H3, H4, and H5; Fig. 1). Cd is the calculated depth. σ is one standard deviation.

only one wavelet, analyses have significant error due to noise effects. However, multiscale wavelet tomography strongly reduces the depth error and risk of artifacts. On synthetic signals, reliable depths of groundwater flow or geological structures can be calculated with errors less than 15%, even when noise represents 20% of the signal (Tables 1, 3, and 4). On field signals, where ground complexity is higher, localization of subsurface structures by their geophysical expression (magnetism, electricity, and gravity) can be achieved with a depth error below 26% (Table 5). The accuracy of the depth is mainly a function of complexity of the subsurface, rather than noise level. In addition, structural order and dip angle representing the source structure are well described by the MWT analyses, even with significant noise (Tables 1, 3, and 4). In comparison to 2D analyses, which require more field data to obtain a regular grid, MWT profile analyses require less data across the studied area. Consequently, the computational power to analyze profiles rather than grid data will be significantly less. MWT profile analyses also give more independent results from one analyzed profile to another, leading to better characterization of the source. Thus, with multiscale wavelet tomography, both real and complex wavelet analyses can be an efficient complementary tool prior to traditional modeling of both subsurface structures and groundwater flow.

Acknowledgments

This work was supported by an NSERC Discovery Grant to G. Williams-Jones. We thank J. Zurek, N. Fournier, O. Boulanger, and one anonymous reviewer for their valuable comments and suggestions.

Appendix A. Supporting information

Supplementary data associated with this article can be found in the online version at doi:10.1016/j.cageo.2011.04.005.

References

Boukerbout, H., Gibert, D., 2006. Identification of sources of potential fields with the continuous wavelet transform: two-dimensional ridgelet analysis. Journal of Geophysical Research 111, B07104. doi:10.1029/2005JB004078.
Cooper, G.R.J., 2006. Interpreting potential field data using continuous wavelet transforms of their horizontal derivatives. Computer and Geosciences 32 (7), 984–992.
Fedi, M., 2007. DEXP: a fast method to determine the depth and the structural index of potential fields sources. Geophysics 72 (1), 11–111. doi:10.1190/1.2399452.
Fedi, M., Quarta, T., 1998. Wavelet analysis for the regional-residual and local separation of potential field anomalies. Geophysical Prospecting 46 (5), 507–525.
Finizola, A., Revil, A., Rizzo, E., Piscitelli, S., Ricci, T., Morin, J., Angeletti, B., Mocochain, L., Sortino, F., 2006. Hydrogeological insights at Stromboli volcano (Italy) from geoelectrical, temperature, and CO_2 soil degassing investigations. Geophysical Research Letters 33, L17304. doi:10.1029/2006GL026842.
Gillot, P.Y., Keller, J., 1993. Radiochronological dating of Stromboli. Acta Vulcanologica 3, 69–77.
Goupillaud, P., Grossmann, A., Morlet, J., 1984. Cycle-octave and related transforms in seismic analysis. Geoexploration 23 (2), 85–102.
Grossmann, A., Morlet, J., 1984. Decomposition of hardy functions into square integrable wavelets of constant shape. Siam Journal on Mathematical Analysis 15 (4), 723–736.
Hallinan, S., Brown, G., 1995. Incremental collapse and stratocone growth within a funnel-shaped caldera, Guayabo, Costa Rica. Journal of Volcanology and Geothermal Research 67, 101–122.
Li, Y., Oldenburg, D.W., 1998. 3D inversion of gravity data. Geophysics 63 (1), 109–119.
Martelet, G., Sailhac, P., Moreau, F., Diament, M., 2001. Characterization of geological boundaries using 1-D wavelet transform on gravity data: theory and application to the Himalayas. Geophysics 66, 1116–1129.
Moreau, F., Gibert, D., Holschneider, M., Saracco, G., 1997. Wavelet analysis of potential fields. Inverse Problem 13 (1), 165–178.
Moreau, F., Gibert, D., Holschneider, M., Saracco, G., 1999. Identification of sources of potential fields with the continuous wavelet transform: basic theory. Journal of Geophysical Research 104 (B3), 5003–5013.
Mauri, G., Williams-Jones, G., Saracco, G., 2010. Accurately determining the depths of hydrothermal systems by self-potential and multi-scale wavelet tomography. Journal of Volcanology and Geothermal Research 191 (3–4), 233–244. doi:10.1016/j.jvolgeores.2010.02.004.
Sailhac, P., Galdeano, A., Gilbert, D., Moreau, F., Delor, C., 2000. Identification of sources of potential fields with the continuous wavelet transform: complex wavelets and application to aeromagnetic profiles in French Guiana. Journal of Geophysical Research 105 (B8), 19455–19475.

Sailhac, P., Marquis, G., 2001. Analytic potentials for the forward and inverse modeling of SP anomalies caused by subsurface fluid flow. Geophysical Research Letters 28 (9), 1851–1854.

Saracco, 1994. Propagation of transient waves through a stratified fluid medium: wavelet analysis of a non asymptotic decomposition of the propagator. Journal of the Acoustical Society of America 95 (3), 1191–1205.

Saracco, G., Labazuy, P., Moreau, F., 2004. Localization of self-potential sources in volcano-electric effect with complex continuous wavelet transform and electrical tomography methods for an active volcano. Geophysical Research Letters 31 (12), L12610. doi:10.1029/2004GL019554.

Saracco, G., Moreau, F., Mathé, P.-E., Hermitte, D., Michel, J.-M., 2007. Multi-scale tomography of buried magnetic structures: its use in the localization and characterization of archeological structures. Geophysical Journal International 1, 87–103.

Tchamitchian, P., 1989. Wavelets and Cauchy-integral on Lipschitz-curves. Annals of Mathematics 129 (3), 641–649.